Polycrystalline silicon ring resonator photodiodes in a bulk complementary metal-oxide-semiconductor process

Karan K. Mehta,[1,*] Jason S. Orcutt,[1] Jeffrey M. Shainline,[2] Ofer Tehar-Zahav,[3,5] Zvi Sternberg,[3] Roy Meade,[4] Miloš A. Popović,[2] and Rajeev J. Ram[1]

[1]*Department of Electrical Engineering and Computer Science and Research Laboratory of Electronics, Massachusetts Institute of Technology, 77 Massachusetts Avenue, Cambridge, Massachusetts 02139, USA*

[2]*Department of Electrical, Computer, and Energy Engineering, University of Colorado Boulder, 1111 Engineering Drive, Boulder, Colorado 80309, USA*

[3]*Micron Semiconductor Israel, 11 Ha'avatz Street, Kiryat Gat 82109, Israel*

[4]*Micron Technology, Inc., Process R&D, 8000 S. Federal Way, Boise, Idaho 83716, USA*

[5]*Intel Israel (74) LTD., P.O. Box 1659, Matam Industrial Park, Haifa 31015, Israel*

**Corresponding author: karanm@mit.edu*

Received October 18, 2013; revised December 19, 2013; accepted January 2, 2014; posted January 14, 2014 (Doc. ID 199248); published February 14, 2014

We present measurements on resonant photodetectors utilizing sub-bandgap absorption in polycrystalline silicon ring resonators, in which light is localized in the intrinsic region of a $p+/p/i/n/n+$ diode. The devices, operating both at $\lambda = 1280$ and $\lambda = 1550$ nm and fabricated in a complementary metal-oxide-semiconductor (CMOS) dynamic random-access memory emulation process, exhibit detection quantum efficiencies around 20% and few-gigahertz response bandwidths. We observe this performance at low reverse biases in the range of a few volts and in devices with dark currents below 50 pA at 10 V. These results demonstrate that such photodetector behavior, previously reported by Preston *et al.* [Opt. Lett. **36**, 52 (2011)], is achievable in bulk CMOS processes, with significant improvements with respect to the previous work in quantum efficiency, dark current, linearity, bandwidth, and operating bias due to additional midlevel doping implants and different material deposition. The present work thus offers a robust realization of a fully CMOS-fabricated all-silicon photodetector functional across a wide wavelength range.

OCIS codes: (130.3120) Integrated optics devices; (130.3990) Micro-optical devices; (040.5160) Photodetectors.
http://dx.doi.org/10.1364/OL.39.001061

Efficient and fast modulation and photodetection represent the most basic active electro-optical functionalities required for a photonic interconnect; in the context of scaled complementary metal-oxide-semiconductor (CMOS) photonic interconnects [1], clear advances have been made in the design and CMOS implementation of free carrier dispersion-based resonant modulators ([2,3] constitute recent examples), but demonstrations of high-quality CMOS photodetectors at wavelengths guided by Si lag behind. Despite impressive demonstrations of both custom-fabricated devices [4,5] and silicon germanium photodetectors monolithically integrated with CMOS receiver circuitry [6], high-quality implementation of photodetectors relying on band-to-band absorption in CMOS has proven difficult due to complications arising from the needed introduction of a low-bandgap material, usually germanium.

Low-loss waveguides can be achieved in the patternable polycrystalline silicon (pSi) gate layer of bulk processes [7]; here the grain boundaries tend to result in larger propagation losses than in crystalline waveguides, some of which is due to absorption on electronic transitions involving grain boundary defect states at energies within the bandgap. This has been observed to generate free carriers, and though waveguide losses on the order of only a few decibels per centimeter might seem to demand very long structures for efficient detection, use of a resonant structure has been shown to allow this low loss rate to give high quantum-efficiency (QE) photodetection in a micrometer-scale device [8]. In crystalline Si as well, defects generated for example through ion implantation have enabled high-performance photodetectors [9] and in resonant configurations as well [10]. The defect-state approach to photodetection is appealing in its simplicity, requiring only silicon and no additional materials; pSi is the natural choice for the waveguide and detector material in bulk CMOS processes, and it furthermore obviates the need for implantation-based defect generation.

In this work we consider ring resonator photodetectors implemented in the pSi of a bulk CMOS dynamic random-access memory emulation process operating both at $\lambda = 1280$ and 1550 nm; as compared to the previous realization [8], these devices include p and n midlevel implants in a $p+/p/i/n/n+$ structure, which allows placement of dopants closer to the core without introducing large losses, which along with particular material deposition allows for more efficient carrier extraction; dark currents are also significantly reduced in these devices as well.

An optical micrograph of one of the finished structures as tested is shown in Fig. 1(a); designed ring resonator ridge widths were 340 and 480 nm for the devices designed at 1280 and 1550 nm, respectively, and ring diameters were 14.5 and 17.5 μm, to limit radiative leakage from the 225-nm-thick core into the ~85-nm-thick contact wings [see cross section in Fig. 1(b)]. The i-region width w_i (as labeled in the schematic) is 700 nm for both devices, and the distance between $n+$ and $p+$ regions $w_m = 1.64$ μm ($\lambda = 1280$ nm) and 1.71 μm ($\lambda = 1550$ nm). The inset shows also a transmission electron

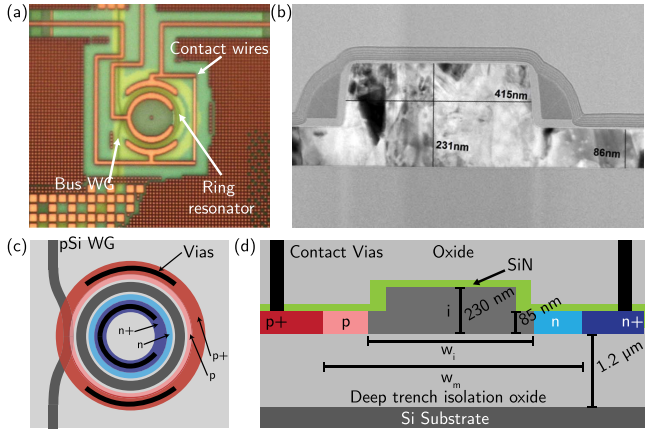

Fig. 1. (a) Optical micrograph of detector device, (b) TEM image of a waveguide cross section, (c) top-down schematic of device showing waveguide and implant geometry, and (d) schematic cross section of waveguide core in ring photodetectors showing intrinsic, mid (p, n), and high-level ($p+$, $n+$) doped regions.

microscope (TEM) image of the final pSi, following all processing steps, which included a chemical–mechanical polish step to reduce top surface scattering [7] and a final crystallization anneal at 950°C anneal for approximately 30 s. The rings were coupled to a bus waveguide, and transmission of the fundamental quasi-TE mode was measured on the through port. Grating structures both at input and output couple light from the on-chip waveguide to nearly-surface-normal oriented cleaved fibers. No drop port was included, and gaps between the bus and ring ridge waveguides were chosen to give near-critical coupling; as shown in Fig. 2, extinction in the through-port transmission of the devices was approximately 11 dB near the device operating at 1280 nm

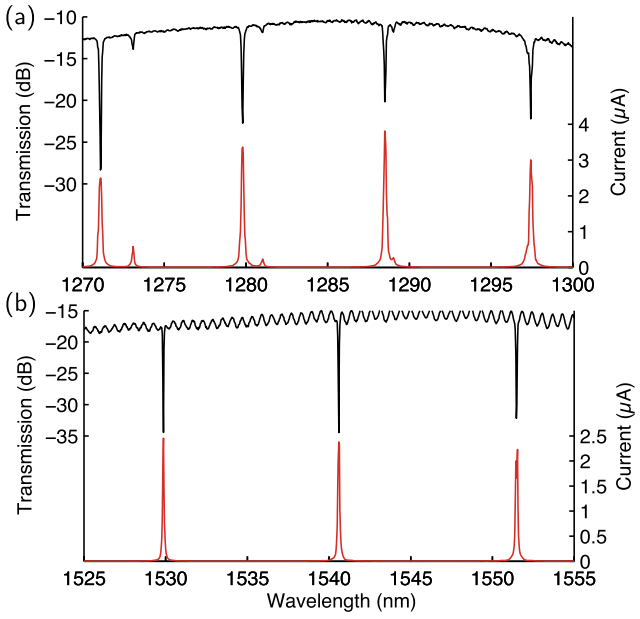

Fig. 2. Fiber–fiber transmission and photocurrent spectra through devices operating near (a) 1280 and (b) 1550 nm, with −1 V bias applied and approximately 80 μW optical power propagating to the device in the input fiber before the input grating coupler.

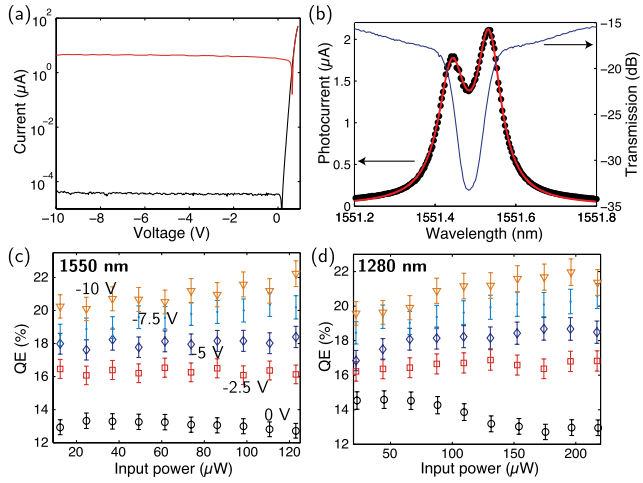

Fig. 3. (a) Illuminated (red) and dark (black) I–V curves for devices at 1280 nm; dark I–V sensitivity is limited to approximately 30 pA by the source-measure unit used [11] and (b) photocurrent and through-port transmission spectra around resonance in the 1550 nm device (black points), along with fit to model calculation for cavity stored energy in the presence of coupled counterpropagating modes (red line). (c) Peak QEs on resonance as a function of in-waveguide input power at five different biases applied to the device operating at 1550 nm, and (d) same data for the device at 1280 nm. Error bars correspond to ±0.15 dB coupling uncertainty.

and 16 dB at 1550 nm. Measured photocurrents are proportional to the intracavity energy, and thus peaks around each resonance are observed, as shown in red in Fig. 2. The measured loaded quality factors are 7000 and 20,000 for the 1280 and 1552 nm resonances, respectively.

Dark currents of both devices were below 50 pA for voltages up to −10 V, significantly below the on-resonant photocurrent even at modest powers. Figure 3(a) shows the dark and illuminated I–V in the 1280 device, with 22 μW input after the grating coupler (I–V characteristics of the 1550 device were nearly identical). We define the peak QE to be $I(\lambda)_{\max}/P_{\text{in}} \times h\nu/e$, where $I(\lambda)_{\max}$ is the maximum photocurrent around the resonance and P_{in} is the input power accounting for insertion loss through the input grating coupler. In the 1550 nm device a peak splitting owing to scattering-induced coupling of the counterpropagating ring modes was observed [12]; measured points from the 1550 nm device are plotted as black dots in Fig. 3(b), with a fit to an expression for total stored cavity energy (in modes of both propagation directions), as derived from coupled mode theory [13]. This was a much smaller effect in the 1280 nm device, where the double peaks were not resolved, and photocurrent spectra were approximately Lorentzian (the secondary peaks visible in Fig. 2 could not be fit with the theory but are consistent with weak cross-polarization excitation, owing to the vertical asymmetry introduced by the pSi contact wings, of a distinct TM-like resonant mode in the ring).

Figures 3(c) and 3(d) plot the measured peak QEs as defined above as a function of power at 0, 2.5, 5, 7.5, and 10 V reverse bias applied, in which error bars represent a ±0.15 dB uncertainty in input coupling. Compared to previous detectors in pSi [8,14], in general, no

power-dependent decrease in QE is observed, perhaps due to higher extraction efficiency, which makes negligible certain density-dependent dynamics. To assess the role of the resonator in these devices we note that as the waveguide loss in these samples was approximately 20 dB/cm at 1280 nm, a straight waveguide section with length equal to the circumference of the 1280 detector studied here would induce only 0.1 dB optical loss, corresponding to a 2.3% bound on maximum QE, assuming that all loss events generate free carriers, along with perfect extraction.

The coupling between forward- and backward-propagating modes, manifested in the double-peaked resonance clearly observed in the 1550 nm device, adversely affects the measured QE due to the fact that the backward-propagating wave in the ring results effectively in a reflection into the bus. As a result, although the measured through-port extinction is large, a significant fraction of the input optical power is not dropped into the cavity; in the absence of this intermodal coupling-induced reflection, peak stored energy and hence total QE (calculated with the same loss rate and coupling as fit to the data, except with intermodal coupling set to 0) would be about 50% higher than observed in measurements on this device presented here.

Response bandwidth of the detectors was characterized by measuring the RF power in the photocurrent signal when illuminated with on-resonance light modulated by the output of a microwave signal synthesizer. Devices were probed with a 40 GHz, unterminated ground–signal–ground probe. The received RF power, relative to that received by a control photodiode with a known flat frequency response, is shown in Fig. 4(a) for the 1280 nm device at 0, 4 and 10 V DC reverse bias applied.

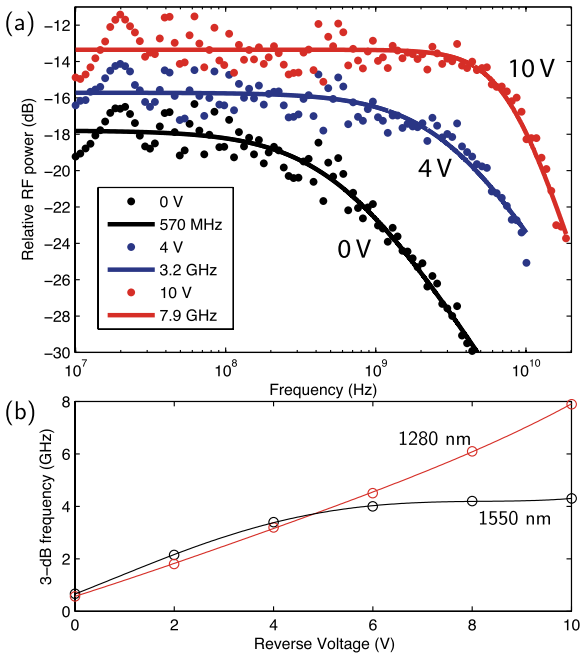

Fig. 4. (a) Measured modulation responses in the 1280 nm detector at 0, 4, and 10 V reverse bias applied. Empirical fits along with the fit 3 dB rolloff are indicated in the legend. (b) Fit 3 dB rolloff frequency as a function of reverse bias voltage for both 1280 and 1550 nm devices (lines are a guide to the eye).

For the purposes of extracting a 3 dB rolloff frequency from the data, which include oscillations over small frequency ranges due to microwave reflections from the high impedance device, the data are presented along with empirical fits of the form $P_{rf} = (P_0/(1 + (f/f_0)^{\alpha}))$ where f_0 is the 3 dB frequency and α and P_0 are fitting parameters.

The response is observed to be consistently flat at low frequencies, with f_0 in general rising with applied DC reverse bias. As shown in Fig. 4(b), the 1280 nm device has a 3 dB frequency that increases roughly linearly with applied bias, consistent with a transit-time limited modulation response, as seen previously in such detectors [14]; however, the mobility in the thicker contact wings here is expected to be higher, consistent with the higher bandwidth at lower bias as compared to [14]. The 1550 nm devices bandwidth ceases to increase after ~6 V, perhaps due to a lower RC limit in that device as compared to the 1280 nm device.

The linearity in photocurrent with respect to input power in these devices makes it simple to achieve tens of microamps of photocurrent, important for triggering practical receive circuits at a high bitrate. The wavelength flexibility also compares favorably to SiGe, where high Ge mole fractions are required to absorb $\lambda =$ 1550 nm light. The QE, though higher than previously reported in such detectors, is not yet at a fundamental material limit; lower sidewall roughness, which could be achieved presently through use of existing processes with higher resolution photolithography, would reduce scattering loss and improve QE both by reducing the mode splitting (and hence increasing the power coupled into the ring) observed in the 1550 nm device as well as increasing the fraction of loss due to absorption relative to scattering out of the ring. We note that the use of resonant enhancement here introduces the need for the same thermal tuning approaches developed for resonant silicon photonic modulators and filters [1,2], which can be a drawback for resonant as compared to nonresonant photodetectors. Nevertheless, the dark current, bandwidth, and QE demonstrated in the present all-Si device are compelling for practical application. Together with demonstrated circuits, and modulators [15] and passive components in the same pSi layer, these devices complete a basic set of optical components enabling a complete photonic communications link in a bulk CMOS process.

This work was supported by DARPA under the POEM program. Karan K. Mehta acknowledges support from a DOE Science Graduate Fellowship. The views expressed are those of the author and do not reflect the official policy or position of the Department of Defense or the U.S. Government. Approved for Public Release, Distribution Unlimited.

References and Note

1. C. Batten, A. Joshi, J. Orcutt, A. Khilo, B. Moss, C. W. Holzwarth, M. A. Popovic, H. Li, H. I. Smith, J. L. Hoyt, F. X. Kärtner, R. J. Ram, V. Stojanović, and K. Asanović, IEEE Micro **29**, 8 (2009).
2. J. M. Shainline, J. S. Orcutt, M. T. Wade, K. Nammari, B. Moss, M. Georgas, C. Sun, R. J. Ram, V. Stojanović, and M. A. Popović, Opt. Lett. **38**, 2657 (2013).

3. E. Timurdogan, C. M. Sorace-Agaskar, E. S. Hosseini, and M. R. Watts, J. Lightwave Technol. **31**, 3907 (2013).
4. S. Assefa, F. Xia, and Y. A. Vlasov, Nature **464**, 80 (2010).
5. L. Vivien, A. Polzer, D. Marris-Morini, J. Osmond, J. M. Hartmann, P. Crozat, E. Cassan, C. Kopp, H. Zimmermann, and J. M. Fédéli, Opt. Express **20**, 1096 (2012).
6. M. Georgas, J. Orcutt, R. J. Ram, and V. Stojanovic, IEEE J. Solid-State Circuits **47**, 1693 (2012).
7. J. S. Orcutt, S. D. Tang, S. Kramer, K. Mehta, H. Li, V. Stojanović, and R. J. Ram, Opt. Express **20**, 7243 (2012).
8. K. Preston, Y. H. D. Lee, M. Zhang, and M. Lipson, Opt. Lett. **36**, 52 (2011).
9. M. Geis, S. Spector, M. Grein, J. Yoon, D. Lennon, and T. Lyszczarz, Opt. Express **17**, 5193 (2009).
10. J. Doylend, P. Jessop, and A. Knights, Opt. Express **18**, 14671 (2010).
11. An approximately –30 pA offset was present in the current source-measure unit used in these I–V measurements; at –10 V, for example, currents of –40 pA were observed in the data in Fig. 3(a) while later measurements with a more sensitive semiconductor parameter analyzer on devices of the same design on a different die yielded currents around –10 pA at the same voltage.
12. B. E. Little, J.-P. Laine, and S. T. Chu, Opt. Lett. **22**, 4 (1997).
13. M. Popović, "Theory and design of high-index-contrast microphotonic circuits," Ph.D. thesis, Massachusetts Institute of Technology, 2008.
14. K. K. Mehta, J. S. Orcutt, O. Tehar-Zahav, Z. Sternberg, R. Bafrali, R. Meade, and R. J. Ram, Sci. Rep. **4**, 4077 (2014).
15. J. M. Shainline, J. S. Orcutt, M. T. Wade, K. Nammari, O. Tehar-Zahav, Z. Sternberg, R. Meade, R. J. Ram, V. Stojanović, and M. A. Popović, Opt. Lett. **38**, 2729 (2013).